

**The TurbEFA Field Experiment - Measuring the Influence of a Forest
Clearing on the Turbulent Wind Field**

Queck, R.; Bernhofer, C.; Bienert, A.; Schlegel, F.;

Originally published:

April 2016

Boundary-Layer Meteorology 160(2016)3, 397-423

DOI: <https://doi.org/10.1007/s10546-016-0151-z>

Perma-Link to Publication Repository of HZDR:

<https://www.hzdr.de/publications/Publ-23548>

Release of the secondary publication
on the basis of the German Copyright Law § 38 Section 4.

The TurbEFA Field Experiment—Measuring the Influence of a Forest Clearing on the Turbulent Wind Field

Ronald Queck¹ · Christian Bernhofer¹ ·
Anne Bienert²  Fabian Schlegel³

Abstract Forest ecosystems play an important role in the interaction between the land surface and the atmosphere. Measurements and modelling efforts have revealed significant uncertainties in state-of-the-art flux assessments due to spatial inhomogeneities in the air-flow and land surface. Here, a field experiment is used to describe the turbulent flow across a typical Central European forest clearing. A three-dimensional model of the inhomogeneous forest stand was developed using an innovative approach based on terrestrial laser-scanner technology. The comparison of the wind statistics of two measurement campaigns (5 and 12 months long) showed the spatial and temporal representativeness of the ultrasonic anemometer measurements within the canopy. An improved method for the correction of the vertical velocity enables the distinction between the instrumental offsets and the vertical winds due to the inclination of the instrument. Despite a 13 % fraction of deciduous plants within the otherwise evergreen canopy, the effects of phenological seasons on the velocity profiles were small. The data classified according to the wind speed revealed the intermittent nature of recirculating air in the clearing. Furthermore, the development of sub-canopy wind-speed maxima is explained by considering the velocity moments and the momentum equation (including measurements of the local pressure gradient). Clearings deflect the flow downward and feed the sub-canopy flow, i.e., advective fluxes, according to wind speed and, likely, clearing size, whereas local pressure gradients play an important role in the development of sub-canopy flow. The presented dataset is freely available at the project homepage.

Electronic supplementary material The online version of this article (doi:[10.1007/s10546-016-0151-z](https://doi.org/10.1007/s10546-016-0151-z)) contains supplementary material, which is available to authorized users.

✉ Ronald Queck
ronald.queck@tu-dresden.de

¹ Institute of Hydrology and Meteorology, Technische Universität Dresden, 01062 Dresden, Germany

² Institute of Photogrammetry and Remote Sensing, Technische Universität Dresden, Dresden, Germany

³ Institute of Fluid Mechanics, Technische Universität Dresden, Dresden, Germany

Keywords Forest inhomogeneity · Metström · Momentum balance · Turbulence measurements · Vegetation model

1 Introduction

General problem and motivation The flow over typical tall forests with clearings, paths and varying topography can be considered as in a permanent transition adapting to the changing surface conditions. Thus, the interaction between the multilayer plant canopies and the atmospheric boundary layer is difficult to capture but, nevertheless, of considerable interest for the assessment of the exchange of atmospheric trace gases (including CO₂) and of storm damage risks.

Advective fluxes within and above a forest canopy occur as a result of the heterogeneity of the soil conditions, the vegetation composition, but also secondary circulations, and produce remarkable uncertainties in the measured fluxes (Aubinet 2008; Feigenwinter et al. 2008; Foken et al. 2011). Heterogeneities in the terrain and canopy structure lead to the development of internal boundary layers with irregular turbulence characteristics (Jegede and Foken 1999), where coherent structures interfere systematically with the vertical exchange of energy and mass (Finnigan 2000; Bohrer et al. 2009). The direction of the total transport and the partitioning of turbulent and non-turbulent fluxes change not only with meteorological conditions (e.g., radiation, wind speed and direction) but also with canopy composition.

Despite the advance in knowledge of the flow within and above tall canopies (see, for example, Gash 1986; Raupach et al. 1987, 1996; Liu et al. 1996; Flesch and Wilson 1999; Finnigan 2000; Lee 2000; Albertson et al. 2001; Huang et al. 2011; Foken et al. 2011; Belcher et al. 2012) many questions remain unanswered. In addition to other issues, description of the spatial development of the wind field within canopies is challenging, as it is a prerequisite for the calculation of energy and mass budget of a control volume in a forest canopy. The problem includes, (i) the effects of typical inhomogeneities, such as small forest clearings and tree-fall gaps, (ii) the development of a secondary wind maximum within the trunk space, and (iii) the relationship between wind speed, drag coefficient, and plant area distribution.

Attempts to model the interaction between the atmosphere and tall canopies are usually based on simplified vegetation structures (e.g., Wilson and Flesch 1999; Shaw and Patton 2003; Yang et al. 2006a; Cassiani et al. 2008; Dupont and Brunet 2008; Sogachev et al. 2008; GavriloV et al. 2010; Huang et al. 2011; Dupont et al. 2011; Banerjee et al. 2013; Kanani-Sühring and Raasch 2015). Particular investigations of the small-scale horizontal inhomogeneity have shown the importance of detailed information on vegetation structure (e.g., Albertson et al. 2001; Bohrer et al. 2009).

Nevertheless, a three-dimensional (3D) vegetation description is not easy to obtain, and even large field experiments, e.g., at Camp Borden (Shaw et al. 1988), Harwood Forest (Irvine et al. 1997), the Hotchkiss River Flesch and Wilson (1999), the ADVEX¹ campaign (Feigenwinter et al. 2008), EGER², (Serafimovich et al. 2011), CHATS³ (Patton et al. 2011), and Le Bray site (Dupont et al. 2011), rarely provide it. Very recently, Maurer et al. (2015)

¹ ADVEX: The extensive experimental activities of the CarboEurope-Integrated Project (CE-IP) advection group took into account the 3D aspects of the problem.

² EGER: ExchanGE processes in mountainous Regions.

³ CHATS: Canopy Horizontal Array Turbulence Study experiment.

presented an exception, studying the effects of the canopy structure on canopy-atmosphere interactions at the UMBS⁴ flux site.

Thus, well-documented field experiments that include meteorological measurements and data on vegetation structure are a prerequisite for the further development of models and the analysis of the energy and mass exchange (Finnigan 2000; Foken et al. 2011).

Objectives The field experiment was conducted within the interdisciplinary project ‘*Turbulent Exchange processes between Forested areas and the Atmosphere*’ (TurBEFA). In contrast to the studies mentioned above, we applied an innovative terrestrial laser-scanning method to record 3D vegetation structure. Laser scanning is a rapidly developing technology that provides a feasible means of obtaining a detailed description of the vegetation for use in numerical models (Bienert and Maas 2009; Vosselman and Maas 2010; Bienert et al. 2010; Queck et al. 2012; Eysn et al. 2013).

Previous TurBEFA publications introduced the TurBEFA field measurements and have shown the benefit of precise vegetation models for numerical simulations (Schlegel et al. 2012; Queck et al. 2015; Schlegel et al. 2015). Further details on the field measurements can be found in the supplementary material of the present article.

Within this contribution, we focus on, (i) the data quality, especially the vertical velocity and the reproducibility of the measurements (Sect. 5), (ii) the classification of the data with respect to meteorological conditions and phenology (Sect. 6), and (iii) the development of wind profiles across and downstream of a forest clearing, the velocity moments, and the momentum budget (Sect. 7). The concluding discussion concerns the effects of forest structure on advective fluxes. The data are part of a reference dataset available at the project homepage.⁵ Technical details of the access are described within the supplementary material.

2 Site

We refer to the *Fluxnet* site *Anchor Station Tharandt* (Baldocchi et al. 2001, www.fluxdata.org), located approximately 15 km south-west of Dresden in Germany (50°57′49″N, 13°34′01″E, 380 m a.s.l.). The site is embedded within a large forested area the ‘Tharandter Wald’ (7120 ha), and comprises a 42-m measurement tower within the forest but also a forest clearing of 50 m × 90 m, called ‘Wildacker’, which is surrounded by coniferous forest stands presenting a typical mid-European forest structure. The average terrain inclination around the site is about 6 %.

Flux measurements began in 1995, and since then an extensive suite of meteorological, hydrological, and ecological measurements, and remote sensing observations have been used to investigate the climate and the exchange processes in and above the forest (e.g., Frühauf et al. 1999; Bernhofer et al. 2003, 2011; Feigenwinter et al. 2004; Grünwald and Bernhofer 2007; Moderow et al. 2007; Schwärzel et al. 2009; Queck et al. 2012; Eysn et al. 2013; Moderow and Bernhofer 2014). Footprint investigations (not regarding the small-scale vegetation structure) have shown that the site is reasonably homogeneous, with fluxes representative of the spruce-dominated area around the *Fluxnet* tower (Rebmann et al. 2005).

⁴ UMBS: University of Michigan Biological Station in northern, lower Michigan, USA.

⁵ Project homepage: <http://tu-dresden.de/turbefa>.

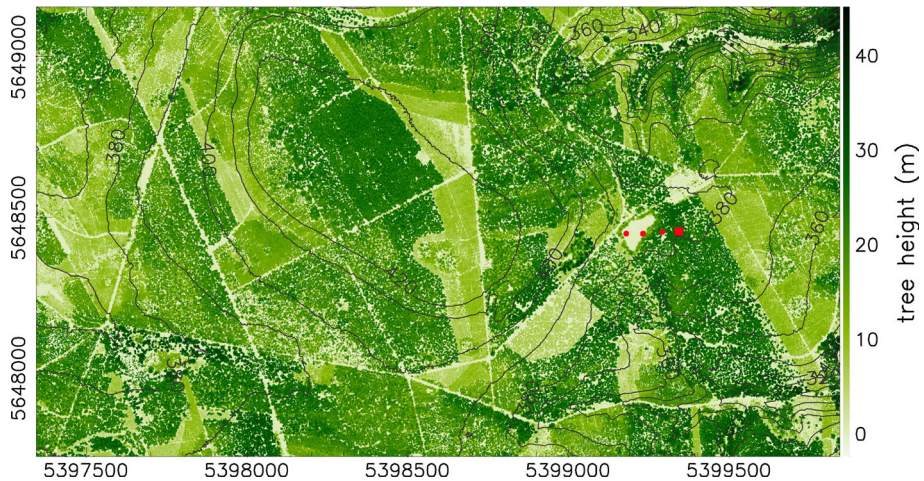


Fig. 1 Map of the site, calculated from airborne laser-scanner data with a resolution of 2 m. The data were recorded in spring 2006 (ATKIS®–DGM2 © Staatsbetrieb Geobasisinformation und Vermessung Sachsen 2013). Tree heights are shown as shading and the digital terrain model as black 10-m contour lines. The axes are labelled with Gauß–Krüger coordinates in m (eastings from the fifth 3° meridian). The *Fluxnet* tower is located at easting 5399344, northing 5648455 and is symbolized by the square. The dots to the left of the square represent the additional towers in place during TurbEFA experiment. The elevated area in the middle of the site is called *S-Berg*

3 Assessment of the Vegetation Structure

Plant Cover The spruce stand around the *Fluxnet* tower was seeded in 1887 and is composed of 87 % coniferous evergreen (72 % *Picea abies*, 15 % *Pinus sylvestris*) and 13 % deciduous (10 % *Larix decidua*, 1 % *Betula spec.* and 2 % others). The stand is characterized by a dense canopy of the mature spruce stand and an open trunk space with a sparse understorey (patches of replanted *Fagus sylvatica* and a few *Rubus*, *Sorbus aucuparia*, and *Sambucus*). Grasses (mostly *Deschampsia flexuosa*) cover approximately 50 % of the ground within the stand. The Wildacker is bordered by a belt of horse chestnuts (*Aesculus hippocastanum*) that smooths the forest edge and reduces the trunk spacing (Otto 2005).

Canopy Parameter In 2008, the number of trees around the *Fluxnet* tower was 335 per hectare and the tree height ranged between 29 and 33 m. The mean canopy height (h) was estimated to be 31 m, and the mean diameter at breast height, $BHD = 0.36$ m. These data were used in the validation of a canopy height model of the ‘Tharandter Wald’ (Fig. 1). The model is derived from airborne laser scans and has a spatial resolution of 2 m. The airborne laser scans were recorded in spring 2006 (© Staatsbetrieb Geobasisinformation und Vermessung Sachsen 2013) and were manually corrected for windthrows resulting from the storm Kyrill (January 2007).

Plant Area Index (PAI) and Plant Area Density (PAD) The determination of the single-sided plant area index is based on a forest assessment from 1999 (including the harvest and analysis of six Norway spruces). Using continuous in-canopy radiation measurements (since 1996), the change in PAI since 1999 can be calculated, yielding a PAI value around the *Fluxnet* tower of $7.1 \text{ m}^2 \text{ m}^{-2}$ in 2008.

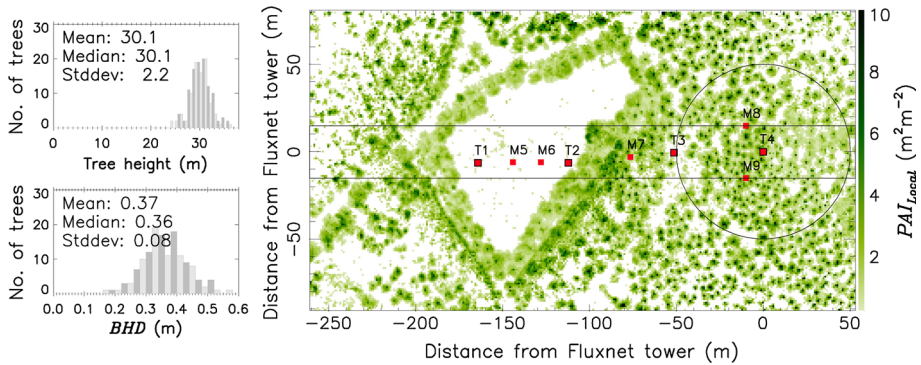


Fig. 2 Map on the *right* vertical integrated plant area density in $\text{m}^2 \text{m}^{-2}$ (PAI_{Local}) derived from terrestrial laser scanning of the section around the towers (resolution 1 m^2). *Small squares* indicate anemometer positions. The *histograms on the left* show the occurrence of tree height and diameter at breast height (BHD) observed within the *circled area* around T4. The area enclosed by the two *horizontal lines* is used for the x - z projections of PAD values in Figs. 5, 9, 10 and 12

Additionally, the plant area was derived from optical measurements in two different ways. In the first approach, we applied the plant canopy analyzer LAI-2000 (LiCOR Biosciences, Lincoln, Nebraska) to measure the gap fraction. In the second and main approach, we applied two terrestrial laser scanners to derive a much more detailed representation of the forest stand around the clearing. The 3D mapping of plant area density covers an area of $330 \text{ m} \times 170 \text{ m}$ with a resolution of 1 m^3 . For a detailed description, see [Bienert et al. \(2010\)](#), [Queck et al. \(2012, 2015\)](#), as well as the supplementary material.

Figure 2 shows the vertical total of the PAD values, with the greatest values observed to the west of the *Fluxnet* tower (T4). Furthermore, the clearing is surrounded by a green belt marking the additional plant area in the lower layers of the stand. A view of a vertical slice (x - z plane) of the derived voxel space is used as the background in Figs. 9, 10 and 13. This vertical slice shows the averaged PAD value over the range $y = (-15, 15 \text{ m})$.

4 Experimental Design and Instrumentation

Wind Measurements We use wind measurements from two experiments. The aim of the first experiment, WinCanop (June 2007–November 2007), was to obtain detailed vertical profiles of wind and air temperature within and above the canopy to optimize the design of the main experiment TurbEFA (May 2008–May 2009). During WinCanop, a vertical array of 13 ultrasonic anemometers/thermometers (hereafter ‘sonics’) was mounted at the *Fluxnet* tower. During TurbEFA, a spatially larger domain including the Wildacker clearing was investigated. The measurement transect was aligned west to east over the clearing according to the predominant wind direction. The set-up includes the *Fluxnet* tower (T4) and three additional towers in the westerly direction (T1, T2 and T3), plus five 2-m masts (M5–M9) in between. Within this framework, the wind vectors were measured at 31 positions (see Figs. 2 and 3). A detailed description of the exact placement and the types of sonics used is provided in the supplementary material. Notably, the sonics at the *Fluxnet* tower were mounted at different positions during TurbEFA and WinCanop.

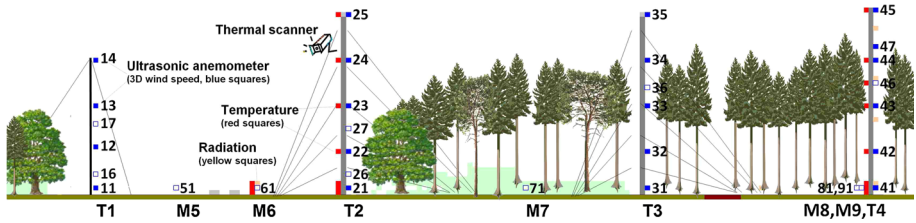


Fig. 3 Schematic site view of the measurement transect in the TurbEFA experiment: the sensor positions are marked by *small squares*. The *filled* and *open blue squares* represent permanent and temporary sonic positions, respectively. Small two-digit numbers identify sonics. The exact positions of the sonics are given in supplementary material, Table 2. The *red squares* mark thermocouple probes. The *green shading* within the trunk space indicates the understorey

Tethered Balloon Soundings The boundary conditions further above the canopy were temporarily investigated using tethered balloon soundings. The intrinsic part of the applied Vaisala DigiCORA Tethersonde System is the Tethersonde TTS111, comprising a cup anemometer and a digital compass for wind measurements, a thin film capacitor for humidity, a capacitive wire for temperature measurements and a silicon pressure sensor.

Pressure Gradient Two “Quad-Disc” static pressure probes (Nishiyama and Bedard 1991) were installed at a height of 1.5 m along the tower transect to measure the horizontal pressure gradient across the forest edge. The first was placed next to tower T2 in the clearing adjacent to the exposed forest edge, and the second was placed within the forest between towers T3 and T4 at $x = -23$ m ($\Delta x = 90$ m). The pressure difference between the probes was measured by a Magnesense[®] MS-121-LCD differential pressure transmitter (Dwyer Instruments, Inc., Indiana, US).

5 Data Processing

Terminology Unless otherwise defined within the following sections, overbars denote time averages (over 30 min), a prime represents departures from time averages and angle brackets denote spatial mean values. The x and y coordinates represent east and north, and z is the vertical coordinate in a right-handed system with the origin at the base of tower T4 (i.e., the *Fluxnet* tower).

The velocity components are u , v , and w , indicating winds from the west, north and below, respectively. The horizontal wind speed is calculated from instantaneous measurements, $u_h = (u^2 + v^2)^{0.5}$, and the friction velocity from covariances, $u_* = (\overline{u'w'^2} + \overline{v'w'^2})^{0.25}$. The variable z indicates the height above the ground, and z_m indicates the measurement height. The thermal stratification of the surface layer is estimated by the stability parameter $\zeta = z_m L^{-1}$, with L being the Obukhov length.

Raw Data Processing The sonic signals were sampled at 20 Hz simultaneously and all raw data were stored. In the post-processing, the data were quality checked, rotated, and combined into 30-min statistics (see Aubinet et al. 2012 and supplementary material). Furthermore, we excluded times with precipitation to avoid artefacts.

Coordinate System One global coordinate system for all measurements is necessary to compare the wind vectors from different anemometers. The two common methods for the rotation

of the measured wind components are called *Double Rotation* and *Planar Fit* rotations (for a description, see Aubinet et al. 2012, among others). Due to the inhomogeneity of the flow field within the canopy, the rationale for the complete *Double Rotation* or *Planar Fit* rotation is not practicable in our case. Furthermore, the definition of the vector basis \mathbf{e}_i by the measured velocity components would preclude comparison of the measurements from different sonics.

In an initial step, we rotated all measurements horizontally, according to the mounting of the single sonics, in one rectangular Cartesian coordinate system aligned to the cardinal directions. According to the set-up of the experiment, we define a velocity vector \mathbf{u} with positive values of the components u , v and w representing winds from the west, north, and below, respectively. A complete rotation in streamlined coordinate systems was applied only for flux calculations from the topmost sensors.

To investigate instrumental errors in the vertical wind component, we utilized the *Planar Fit* rotation (Sect. 6.1). The implied multiple regression of \bar{w} with the horizontal wind components \bar{u} and \bar{v} (Eq. 1) supplies the average inclination of the wind field in the geographic coordinate system (b_1 and b_2 in Eq. 1),

$$\bar{w} = b_0 + b_1\bar{u} + b_2\bar{v}. \quad (1)$$

Often, the error term or bias b_0 is attributed to measurement errors, which need to be corrected. However, the scatter of the measurements influences the calculation of the coefficients and might lead to statistical artefacts in the estimation of the bias b_0 , especially when applied to the data of each wind-direction sector separately. To overcome this problem, we performed a sector-wise fitting but subsequently averaged the estimated b_0 of all sectors. This approach is based on the assumption that the instrumental error does not change with wind direction.

Reference Position, Data Classification, and Averaging The comparison of spatially distributed point measurements or modelling results is often performed via normalization of the data with values at the canopy height. Considering the variability of the canopy heights, this approach is not applicable here; thus, we used the topmost positions instead as the level that is least affected by changes in canopy structure. Furthermore, the values measured at an individual position in a developing internal boundary layer can fluctuate and are not representative for use as a reference. Thus, the mean of the topmost positions from all towers is chosen as the reference indicated by the index ‘*ref*’.

To explore the influence of the meteorological situation on the airflow within the roughness layer, the data are binned into classes according to wind direction, wind speed, friction velocity, and stability. These criteria were calculated from the measurements of tower T4 at a height of 42 m. Calculating the mean values for each class, the measurements were normalized with the reference for each 30-min timestep and then averaged over each class. These variables are indicated by the index ‘*n*’.

We assume that binning measurements from slightly different flow directions but similar meteorological situations is similar to building a spatial average for the sensor position. The chosen size of the wind sectors was 30° , which represents a compromise between the ability to detect the characteristics of the different flow directions and a spatial smoothing of the measurements at one point. Table 1 shows the defined ranges for the binning of the data.

The wind-speed classes were defined using an empirical procedure. We divided the dataset into classes of 0.2 m s^{-1} and plotted profiles of the velocity moments. Trying to find a minimal number of classes that capture the features of the profiles, we combined the data successive

Table 1 Ranges for the data binning

Variable	Segmentation
Stability, ζ	Unstable $< -0.1 < \text{near-neutral} < 0.1 < \text{stable}$
Wind direction (WD)	Sectors of 30°
Wind speed $\overline{u}_h(42 \text{ m})$ (m s^{-1})	0.2 ... 1.5, 2.0 ... 3.0, 3.5 ... 4.5, 5.5 ... 20
Phenology	Spring 2008: 1 May–1 June 2008, developing foliage Summer: 1 June–1 Sept. 2008, fully developed foliage Autumn: 1 Sept.–15 Nov. 2008, partially reduced foliage Winter: 15 Nov. 2008–10 Apr. 2009, defoliated plants Spring 2009: 10 Apr.–1 May 2009, developing foliage
Standard case	No precipitation, $-0.1 < \zeta < 0.1$, $255^\circ < WD < 285^\circ$, $2 \text{ m s}^{-1} < \overline{u}_h < 4 \text{ m s}^{-1}$, $0 < u_* < 1.5 \text{ m s}^{-1}$

into four wind-speed classes. The gaps between the wind-speed classes are introduced to accent the differences between them.

Additionally, we segmented the year according to the phenological phases due to the presence of deciduous trees and understorey (13 % of the plant cover).

6 Data Quality Assessment

6.1 Vertical Wind Component

Accurate calculations of the vertical velocity are uniquely important for the calculation of energy and mass fluxes between the surface and the atmosphere (Lee et al. 2004). The small values of \overline{w} can be severely disturbed by errors in the definition of the coordinate system, by the precision of the anemometers (e.g., Högström and Smedman 2004; Nakai et al. 2006), and by effects of the environment (or set-up) of the sensor, which may result in local disturbances of the wind field. The manufacturers of the utilized ultrasonic anemometers state a resolution of 0.01 m s^{-1} and an accuracy between ± 0.05 and $\pm 0.1 \text{ m s}^{-1}$.

To assess the accuracy of the vertical velocity measurements, we applied a modified *Planar Fit* method (Eq. 1). The resulting intercept b_0 of the regression indicates a vertical wind in the absence of a horizontal wind, which is assumed to be an instrumental bias.

Near the surface, or even within the canopy, we faced two problems associated with the use of this method. Imagine the case where the streamlines of the flow towards a sensor are inclined downwards for all wind directions. A regression using all directions at once could result in an intercept but without requiring an instrumental bias. Therefore, measurements in complex terrain (and undoubtedly some within a canopy) require a sector-wise *Planar Fit* as the inclination of the streamlines changes non-linearly with the flow direction. However, a sector-wise *Planar Fit* often leads to different intercepts for each sector. In other words, in the absence of horizontal velocities, varying vertical velocities were measured by the same sensor, which is not rational considering the negligible flow distortion by the canopy at low wind speeds.

Thus, we fitted planes to the data of each 30° wind sector, but propose to use the average of the resulting intercepts over all wind sectors, $\langle b_0 \rangle$, to correct the vertical velocity. The

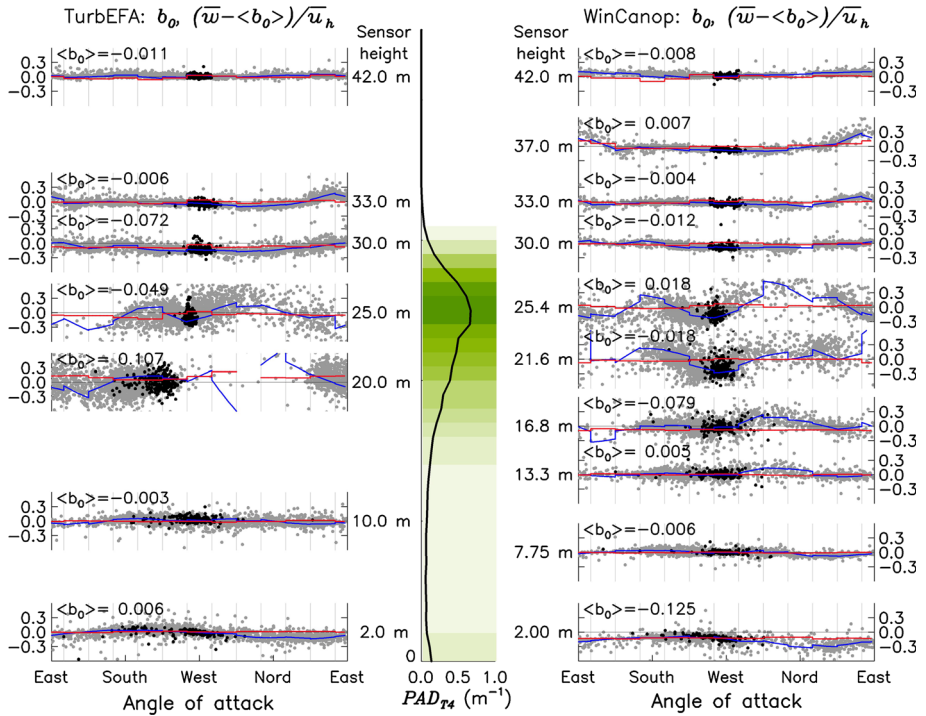


Fig. 4 Normalized vertical velocities versus wind direction at tower T4 from the experiments TurbEFA (*left panel*) and WinCanop (*right panel*, not all sensors are shown). *Dots* show the normalized measured values $(\bar{w} - \langle b_0 \rangle) / \overline{u}_h + \langle b_0 \rangle$, where $\langle b_0 \rangle$ is the mean of intercepts of the *Planar Fit* regressions over all wind sectors. The values of b_0 are plotted as a *red line*. The *blue line* shows the calculated normalized vertical velocity from the regression $b_1 u_1 + b_2 v_1$, where u_1 and v_1 indicate the components of a wind vector of magnitude 1 m s^{-1} . The difference between the *blue line* and the *red line* is the average of the normalized vertical velocity. Situations with westerly winds at the top-most sensor are marked by *black dots*. The PAD_{T4} is the projected plant area density around tower T4

results are shown in Fig. 4. Independent of the position or type of instrument, we calculated mean instrumental biases of up to 0.12 m s^{-1} , which exceeds the range of the manufacturers by just a few tens of mm s^{-1} .

To illustrate the large effect of this small error in the velocity measurement on the advective fluxes, we can imagine a mean CO_2 concentration difference between the canopy and the free air above of 2 ppm (i.e., $\approx 4 \mu\text{g m}^{-3}$). The determined mean instrumental bias in the vertical velocity could lead to a difference in the yearly advective flux of 10 kg m^{-2} and should be corrected. Sensor positions within the barely turbulent flow below the canopy show an almost constant b_0 ; however, within and above the canopy, the value of b_0 is unsteady. The erratic deviations from $\langle b_0 \rangle$ do not point to the influence of single transducer couples of the sonics as a reason. Rather, we assume that the scatter in the 30-min means of w introduces a larger error into the estimation of b_0 . This feature is smoothed out by the spatial mean of the intercept $\langle b_0 \rangle$. After correction with $\langle b_0 \rangle$, the measurements of \bar{w} in Fig. 5c form almost identical profiles in both experiments.

Figure 4 shows generally similar wind vector inclinations in both experiments; above and below the canopy, the inclinations are small. It becomes clear that the patterns of \bar{w} within the canopy are not regular and are dominated by surrounding trees. Additionally, we observe a

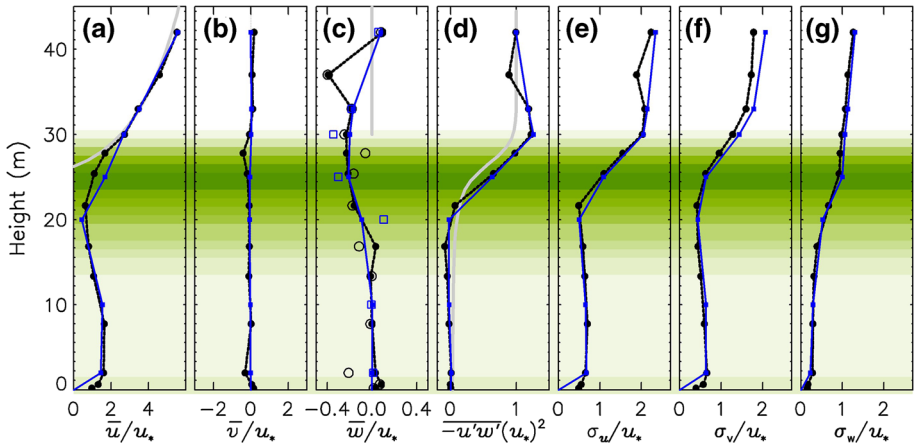


Fig. 5 Comparison of the statistics from the experiments WinCanop (dashed black line with points) and TurbEFA (solid blue line with horizontal marks). The mean profiles are calculated from near-neutral situations with westerly winds between 3.8 m s^{-1} and 4.2 m s^{-1} . The plots show mean values normalized with the friction velocity u_* : **a–c** velocity components (note the different scales of the x -axes for the vertical velocity), **d** Reynolds stress, **e–g** standard deviations of the velocity components. For comparison, theoretical functions of the canopy structure are included: **a** the logarithmic wind profile using a displacement height of 24 m and a roughness length of 2.2 m and **d** the function $\overline{u'w'} = \exp(-0.5PAC)$ according to Yi (2008), where PAC is the cumulative single-sided plant area density

large range of \overline{w} (upwards and downwards) for all flow directions. In contrast, the horizontal velocity components show the dispersive character of the flow around the trees. The sensors at 20 and 25 m in the TurbEFA experiment are obviously located in a wind channel between the trees. Flow from the west sector above the canopy (marked by black dots in Fig. 4) is restricted to a smaller sector in the dense canopy at 25 m and directed to the south-west at 20 m. The corresponding measurements in the trunk space show, on average, a redirection of the airflow from the west again. However, the single data points are spread over a much larger wind sector. These signs of decoupling lead to the conclusion that the flow within the trunk space is mainly driven by the inflow and outflow at the canopy edges.

6.2 Reproducibility of the Measured Profiles

A fundamental principle of scientific investigation is the reproducibility of experimental results. However, the application of this principle to field experiments is limited. Field experiments are influenced by numerous environmental conditions, which are not fully controllable. For single-point measurements in a heterogeneous environment, spatial representativeness is an additional problem. In addition to temporal changes in the environment, small changes in the set-up of two different experiments may lead to a large scatter in the results. In our case, the average vertical distribution of the vegetation dominates the shape of the wind profile, but horizontal inhomogeneities may lead to deviations depending on the position and wind direction.

Within the preliminary experiment WinCanop, we deployed a dense sensor profile of 13 sonics at Fluxnet tower T4 (see Sect. 4). During the TurbEFA we used only seven sonics at T4 in somewhat different vertical and horizontal positions ($\Delta x \approx 2\text{--}6 \text{ m}$) as well as different sonic types. Above the canopy, identical sensor positions were deployed in both experiments, leaving out the 37-m level during TurbEFA. Only the situations that met the

standard case (defined in Table 1) were used for the comparison of the experiments. A total of 252 situations (30-min statistics) were filtered from the TurbEFA dataset, and a total of 114 situations were filtered from the shorter WinCanop dataset.

Figure 5 shows a general conformity between the profiles. We see that the streamwise horizontal velocity profiles above the canopy are well described by a logarithmic function (Fig. 5a). At the 25-m level, the TurbEFA measurements have slightly higher values than those of WinCanop. This ensures that the height of the inflection point in the wind-speed profile, often visible at the top of the canopy, is clearly detectable only in the WinCanop data. Thus, the difference in the horizontal sensor positions between the experiments reveals the horizontal inhomogeneity of the mean canopy flow.

The vertical kinematic stress ($\overline{u'w'}$) in Fig. 5d is less affected by these changes. Within the canopy the decrease in $\overline{u'w'}$ is also reflected well by a function of the cumulative single-sided PAD (grey line in Fig. 5d, see Yi 2008). Of course, the local increase and maximum value of $\overline{u'w'}$ within the roughness layer, which is likely caused by an advective momentum entry, could not be modelled by this function.

The WinCanop measurements at 37 m provide the information that the local maximum in turbulence intensity (see Fig. 5d, e) is constricted to a thin layer at the canopy top and is related solely to the streamwise turbulence. The systematic deviation in the profile of the crosswise standard deviations, σ_v , above the canopy cannot be explained by a different set-up, as the instruments above the canopy were not changed between the experiments. This deviation reveals a greater turbulence intensity during TurbEFA. However, the profiles of σ_u and σ_w (Fig. 5e, g) are almost identical. The measurements at heights 0.5 and 0.2 m show considerable wind speeds and horizontal turbulence near the forest floor, whereas the vertical exchange is limited.

The vertical velocity, \overline{w}/u_* (Fig. 5c), is corrected for the instrumental bias as discussed in the previous sub-section. This procedure removes a large portion of the scatter in the profiles of \overline{w} ; thus, the difference in \overline{w} between the experiments vanishes almost completely after the correction. Both experiments show that \overline{w} , which is approximately zero or slightly positive at 42 m, becomes negative within the roughness layer and in the upper range of the canopy, and decreases again within the trunk space. The additional WinCanop sensor positions show gaps in the coverage of the TurbEFA profile. The increased \overline{w} at 0.65 m is caused by the local slope of the forest floor, while in contrast, the reason for the negative peak of \overline{w} at 37 m is not so obvious. A comparison with Fig. 4 (right panel) shows that the vertical angle of the flow does not change much between 33 and 37 m; consequently, the larger vertical velocity at 37 m results from a general increase in the wind speed between 33 and 37 m.

The small differences between the profiles from both of the experiments may have a larger effect on the assessment of the advective fluxes. Thus, it is very important to have sensors at the local extrema in the PAD profile and near the forest floor. The results show that the measurements are spatially representative for horizontal distances within a range of 1–5 m, i.e., comparable with numerical simulations that apply a comparable grid size.

7 External Conditions of the Turbulence Measurements

7.1 Ambient Flow Characteristics

The general meteorological conditions during the experiments correspond well to the long-term average. The recorded data contain neither extreme events (storms, heavy rains or droughts) nor phenological anomalies. We observed 72 days with complete snow cover and

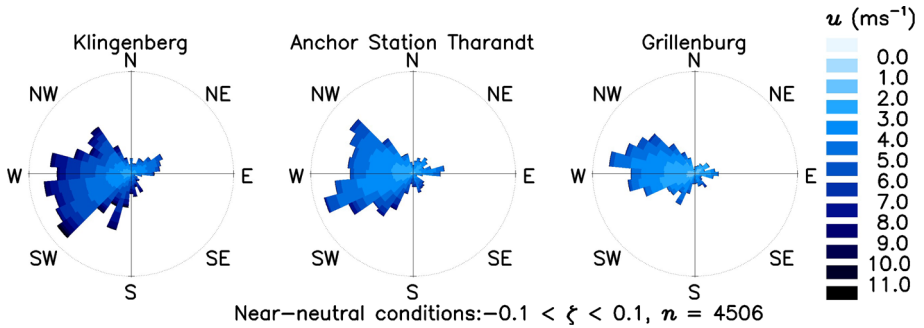


Fig. 6 Distribution of wind speed and direction measured at the top of the Fluxnet tower and at two other measurement sites within the region for whole experimental period (near-neutral stratification only)

54 days with a snow depth >0.1 m, which we assume influences the aerodynamic properties of the forest.

Figure 6 compares the wind distribution of the *Anchor Station Tharandt* with two undisturbed measurement sites, *Klingenberg* (agriculture) and *Grillenburg* (grassland), in the vicinity (a site description is given in Prescher et al. 2010). Prevailing westerlies dominate the wind distribution of all three sites. However, the west wind sector of the *Anchor Station Tharandt* shows somewhat protruding flanks compared to both of the other sites, and furthermore, the strongest winds occur at the flanks. This may indicate the influence of the *Berg* hillock, which is located directly to the west of the site (see Fig. 1). Despite the fact that the measurement transect is in line with the most frequent wind direction, the strongest winds are not covered by the wind sector investigated in this study ($270^\circ \pm 15^\circ$).

Tethered balloon soundings were conducted to support the definition of boundary conditions in numerical models. Figure 7 shows typical vertical profiles for fair weather. For this, the measurements were first binned into height layers of 5 m, and the soundings with similar profiles were then averaged to derive typical profiles. Based on the potential temperature, the soundings can be divided into near-neutral stratification in the afternoon and a more stable stratification during the night. Almost all wind profiles coincide in one characteristic profile form (except the after-dawn profile at 0707 Central European Time). Compared to the theoretical logarithmic wind profile, their more bent shape resembles typical unstable wind profiles. However, the stratification was rather stable, which is a further indication of the influence of the *S-Berg*. The flow over the hill appears to accelerate at levels between 50 m and 250 m.

7.2 Phenological Seasons

A basic assumption of the experiment was that the small cover of deciduous plants (13 %) causes no significant seasonal cycle in the aerodynamic drag of the plant cover. However, the main part of the deciduous plants is located around the clearing and within the trunk space of the mature spruce stand. Hence, we must consider a small *PAI* amplitude of the coniferous evergreen.

During the TurbEFA experiment, leaf unfolding was observed on 21 April and the May shoots were observed on 17 May in 2008 (i.e., the day of year, DOY, 112 and 138, respectively). In 2009, the leaf unfolding took place nine days earlier. To estimate the effect on the *PAI*, we conducted frequent *PAI* measurements in 2013 using a LAI-2000. Figure 8 shows

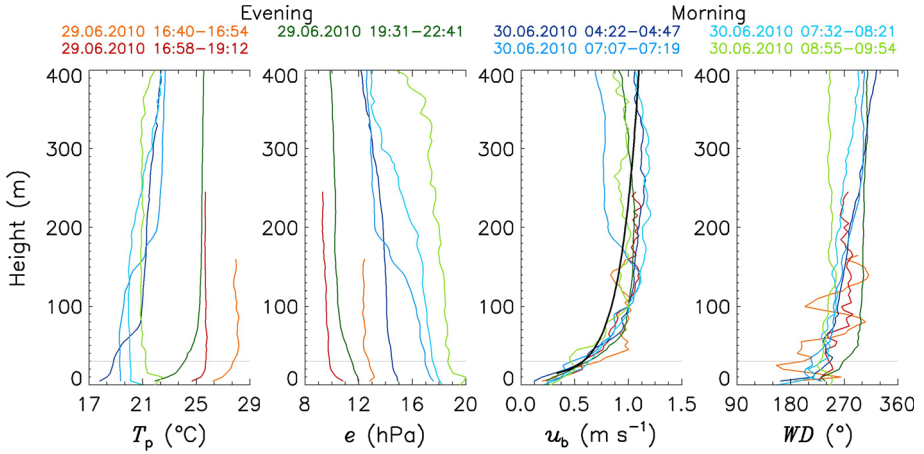


Fig. 7 Typical vertical profiles for fair weather derived from tethered balloon soundings between the evening of 29 June and the morning of 30 June 2010. Times are given in Central European Time. Sunset and sunrise occurred at 2017 and 0402, respectively. From *left to right*, the plots show the potential temperature T_p , water vapour pressure e , wind speed u_b (a theoretical logarithmic wind profile is shown in *black*), and wind direction WD

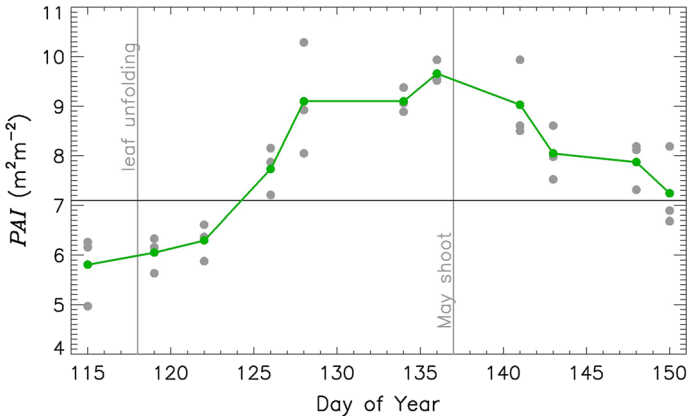


Fig. 8 May shoot and leaf unfolding in the year 2013. The PAI value was derived from gap light analyzer (PCA LAI-2000, LiCOR, Lincoln, Nebraska) by applying a clumping factor of 3.5. On three different measurement grids (10 m \times 10 m, grid size 2 m), 25 samples were taken each time. The *grey dots* symbolize the averages of the measurement grids, and the *line with dots* symbolizes the average over all 75 samples

an increase of more than $3 \text{ m}^2 \text{ m}^{-2}$ around DOY 125 (4 May 2013) but also a decrease in the following twenty days. The difference between winter and summer likely does not exceed $1 \text{ m}^2 \text{ m}^{-2}$. However, the influence of the complete annual cycle has not been measured yet. To investigate the effects on the wind field within the canopy, we divided the dataset into the phenological phases listed in Table 1.

Most of the measurement positions show only small changes during the seasonal cycle. An increased wind speed can be observed during the defoliated winter season at the first level within the trunk space, on the clearing at the second level at T1, and, significantly, in the canopy at tower T3 ($>10\%$). These changes are clearly connected to a change in plant

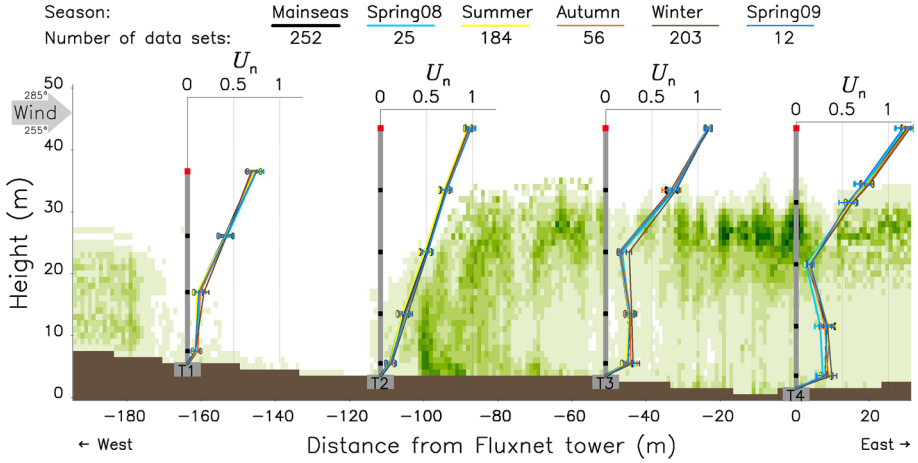


Fig. 9 Normalized mean wind speed $U_n = (\overline{u^2} + \overline{v^2})^{0.5} / \overline{u_{ref}}$ for different seasons (only near-neutral situations with westerly winds). The standard deviation is indicated by *error bars*. The reference positions are marked by the *red dots*. Please note that only the sensors at heights 2, 10, 20, 30 and 40 m, indicated by the *black dots*, are used for the comparison, as they were operated during all seasons. Sensor positions are connected with *lines* for better visibility only, and some features of the profiles within the canopy are not shown by this representation. The *green shading* shows the plant area distribution averaged vertically to the cross-section over a range of ± 15 m

area density. The leaves of the chestnut belt around the clearing influence the measurements at tower T1; most of the other deciduous plants were located between towers T2 and T3. The profiles of the vertical momentum transport (not shown here) reveal a similar pattern. In addition to an increase within the canopy at tower T3 (20 m) during the winter, we observed a small increase at the top of the canopy in spring 2008 and 2009 but not within the canopy.

Thus, we have to consider the influences of seasonal plant development during the spring and the defoliated stage during the winter. For further investigation, we defined a ‘*Main Season*’ that combines the seasons summer and autumn 2008 and spring 2009 (see Table 1). This period represents the foliated stage and corresponds to the laser scans of the canopy.

8 Flow Across the Clearing

8.1 Wind-Speed Dependence

Streamlining The aerodynamic drag on a canopy changes with increasing wind speed. This effect is known as streamlining (Raupach and Thom 1981; Brunet et al. 1994; Finnigan 2000). By implication, we assumed also a change in the shape of the wind profiles with increasing wind speed and investigated the variability in the profiles for different wind-speed classes (defined in Table 1). Despite the relatively long duration of the experiment, the maximum wind speed in the west-wind sector only reached 6.4 m s^{-1} (maximum values registered in other years vary between 10 and 18 m s^{-1}).

In contrast to our assumptions, the profiles of the normalized horizontal and vertical wind components (u_n and w_n , respectively) in Fig. 10 show that all wind-speed classes above $\overline{u_h}(42 \text{ m}) = 2 \text{ m s}^{-1}$ form a single profile pattern. Only the profile of the lowest wind-speed class deviates from the average profile. Directly above and within the canopy, we observe

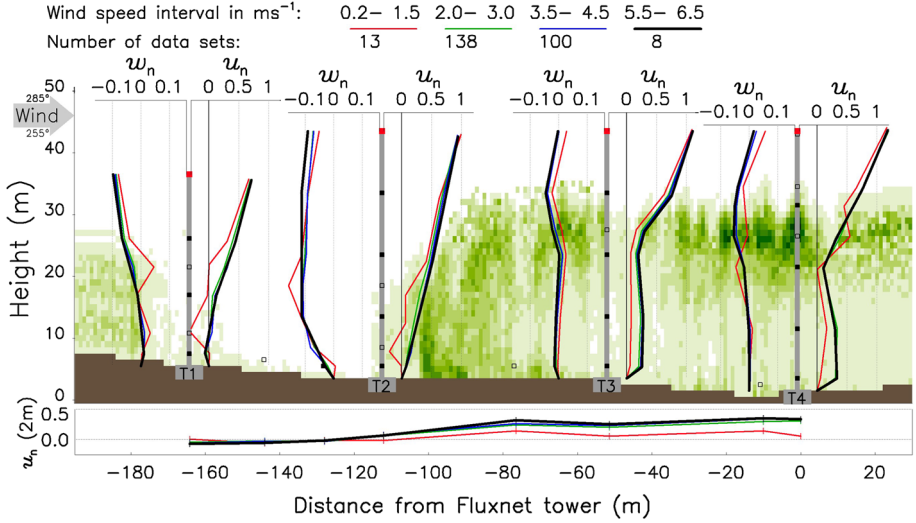


Fig. 10 Normalized mean wind profiles for different classes of horizontal wind speed (only near-neutral situations with westerly winds). The *square symbols* mark the positions of the sensors and the *background* presents the PAD value similar to Fig. 9. The data are classified and normalized with a spatial mean of the horizontal wind speed measured at the *red dots*. The *upper panel* shows the normalized vertical velocity $w_n = \overline{w}/u_{ref}$ on the *left* of each tower and the normalized west wind component on the *right* $u_n = \overline{u}/u_{ref}$ (note the different scales of the *x-axis*). The plot below shows u_n from all positions at 2-m height

lower u_n values and lower w_n values. This indicates that the canopy exerts a higher resistance to the flow or a larger displacement of the flow during low wind speeds.

Rudnicki et al. (2004) reported that the frontal area of tree crowns starts to decrease at wind speeds $>4 \text{ m s}^{-1}$. In our data, a transition is observed only at low wind speeds. Thus, we assume that the old rigid coniferous stand starts to streamline at the unobserved wind speeds $>6 \text{ m s}^{-1}$. Visual observations in the field support this assumption but revealed that the trees start to sway at much lower wind speeds. The swaying increases the turbulent exchange within the canopy and reduces the thickness of the quasi-laminar layer around the conifer shoots. This effect could allow higher wind speeds within the canopy. Furthermore, the motionless canopy elements during low wind conditions might be the reason for the uneven low wind-speed profiles at T4 (increase in u_n within the canopy), as a higher dispersion of the flow occurs within the canopy.

Intermittent Recirculation in the Clearing The differences between the two characteristic shapes of the wind field (distinguished by wind speed $<2 \text{ m s}^{-1}$ and wind speed $>2 \text{ m s}^{-1}$) are even larger in the clearing than within and above the canopy. We observe a separation zone behind the forest-clearing step, from which a rotor-like structure develops over the clearing in situations with lower wind speeds. The profiles of the normalized horizontal velocity component u_n are marked by constant gradients in the clearing, but in the lee of the forest edge at tower T1, u_n decreases to zero at a height of $z \approx 10 \text{ m}$. The vertical velocity component w_n is already negative at the topmost level at tower T1, which is likely caused by the slope of the terrain (Fig. 11). At tower T2, the region of negative w_n has extended downwards into the lowest layer. In the presence of low wind speeds, this airflow feeds a horizontal back-streaming at a height of 5 m and turns into a positive vertical airflow at tower T1, forming a recirculation.

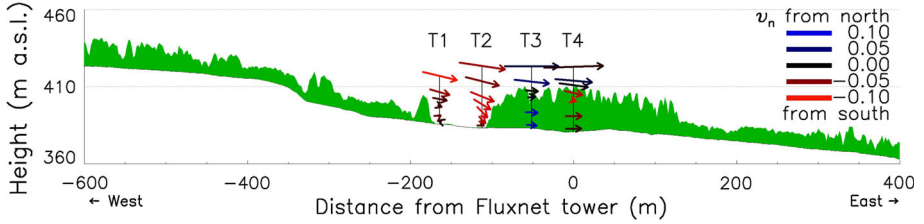


Fig. 11 Mean velocity vectors for near-neutral situations with westerly winds in relation to topography. The length of the vectors shows u_n and w_n relative to the reference velocity, similar to Fig. 10. The colour of the vector represents the lateral velocity $v_n = \bar{v}/u_{ref}$, with red indicating northward motion (into the picture plane) and blue southward motion (out of the picture plane). The terrain and vegetation profile shows a vertical west-east slice of the airborne laser-scanner domain shown in Fig. 1; the vertical dimension is exaggerated two-fold

Although this separation zone shrinks to a smaller region around tower T1 at 30-min wind-speed averages greater than 2 m s^{-1} , we assume that a recirculation arises frequently in the short lulls between higher wind speeds (see also the investigations of Huang et al. 2011). At a wind speed $< 2 \text{ m s}^{-1}$, the momentum is probably too small for the airflow to penetrate the vegetation at the edge of the forest from the clearing. As a result the horizontal velocity in the open trunk space around towers T3 and T4 is relatively low or even negative at tower T3 in a few situations.

The turbulent vertical momentum transfer expresses, with one exception, no significant differences between the wind-speed classes (not shown here; for an average of all wind-speed classes, see Fig. 12). The profiles of the lowest wind-speed class are the only ones to differ from the average profile form. In the clearing, the vertical momentum drops to zero below 15 m at tower T1 and decreases substantially at tower T2. This indicates that the organisation of the airflow to a recirculation is associated with a weak vertical momentum exchange in the clearing.

The decomposition of the wind pattern into direct through-flow (or exit flow) and recirculating flow was proposed by wind-tunnel and numerical studies (e.g., Raupach et al. 1987; Flesch and Wilson 1999; Yang et al. 2006b; Cassiani et al. 2008; Frank and Ruck 2008; Fontan et al. 2012) and observed in a larger clearing by Detto et al. (2008). A new aspect is that the smooth-to-rough surface change has obviously an upwind influence. This becomes more evident by also considering the normalized cross-wind component ($v_n = \bar{v}/u_{ref}$, positive for the wind direction from the north). Figure 11 shows wind vectors averaged over all wind-speed classes; the v_n increases significantly over the clearing, i.e., the flow turns towards the north at T2. This indicates that a spiralling flow over the clearing also occurs at higher wind speeds (clockwise rotation around a horizontal axis from west-south-west to east-north-east). Note that the inflow at the top of tower T1 is already from the south, which again points to an influence of the small upstream hill.

8.2 Velocity Moments

A general view on the airflow over the clearing has already been provided in Queck et al. (2015). Inspired by Raupach et al. (1996), we present here a combined view on the single-point turbulence statistics (Fig. 12) and discuss some features in more detail.

The first view reveals two characteristic profile shapes: rather linear profile forms over the clearing (T1 and T2) and typical s-shaped profile forms within the forest (T3 and T4).

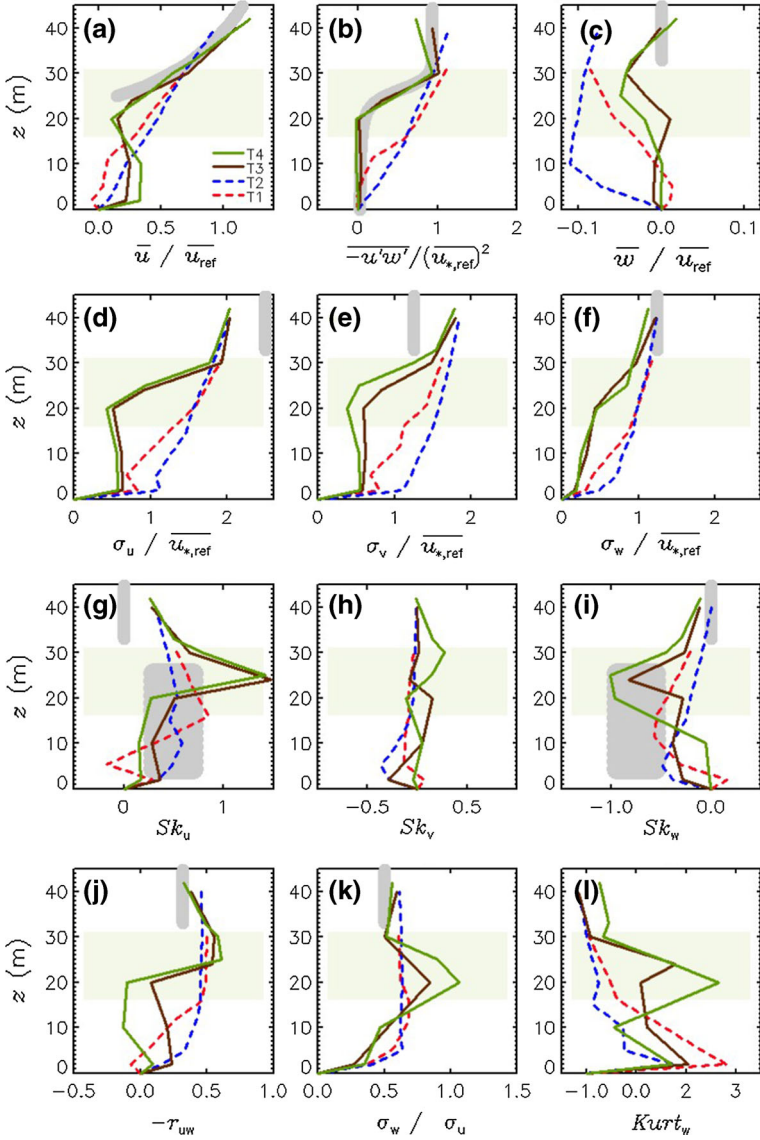


Fig. 12 Velocity moments calculated from measurements at the four towers for near-neutral conditions. The ordinate shows the height above ground. The *grey shading* indicates the known range of turbulence characteristics (see Finnigan 2000, for a review)

Comparing the velocity profiles from the clearing and the forest, we see a deceleration inside the canopy and an acceleration above and below the canopy, as the average flow is squeezed around the denser sections of the canopy (compare also to Fig. 13). Above the canopy, the development of the horizontal velocity field is accompanied by a divergence of the flow; i.e., w_n is slightly positive at a height of 40 m, but negative at canopy height.

The clearing deflects the flow downwards and feeds the airflow below the canopy, supporting a secondary wind-speed maximum there. As discussed in Sect. 8.1, this sub-canopy flow has an onset at a wind speed $\overline{u}_h(42 \text{ m}) \geq 1.5 \text{ m s}^{-1}$. Rather linear velocity profiles and the intensified turbulence over the clearing (Fig. 12b–f) reveal the effect of a mixing zone (Raupach et al. 1996; Lee 2000) that generates enhanced instability and turbulent exchange. Downstream of the forest edge, the shear layer between the two co-flowing streams (within and above the canopy), which was dissolved over the clearing, is re-established rapidly, and the profile at tower T3 shows an inflection point right below the canopy top.

The scale of the active eddies is defined by the maximal vertical gradient of the horizontal wind speed $L_s = u(h)/(\partial \overline{u}(h)/\partial z)$. Typical values are $0.1 h$ and $0.5 h$ for dense and moderate canopies, respectively (Raupach et al. 1996). At towers T3 and T4, we derived comparable small values of $L_s \approx 0.17 h$, which characterize the depth of the turbulent exchange with the canopy.

An interesting feature within the roughness layer is the local maximum of $\overline{u'w'}$ at canopy height. We found a relative increase of this maximum with wind speed, a decrease with friction velocity, and an increase with the stability index $\zeta(42 \text{ m})$ (not shown here). Thus, we assume, $\overline{u'w'}$ increases at the canopy top due to locally generated turbulence and by the organization of the flow according to the canopy structure; the latter is indicated by the increasing correlation coefficient r_{uw} (Fig. 12j).

The horizontal distance for the adjustment of the flow to roughness elements is characterized by the canopy-drag length scale $L_c = (c_d a)^{-1}$. Belcher et al. (2008) reported a distance of around $3L_c$ from the forest edge for the development of the canopy profile. Considering PAD values between 0.2 m^{-1} and 0.6 m^{-1} and local drag coefficients between 0.1 and 0.3 (see Queck et al. 2012), we obtain $L_c \approx 13 \text{ m}$. This leads to an adjustment distance of approximately 40 m, which is smaller than the distance between tower T3 and the clearing. In fact, the similarity of the profiles of towers T3 and T4 (Fig. 12a, b) allows us to assume an almost complete adjustment of the mean flow to the canopy at tower T3.

However, the re-established instability zone around the inflection point of the wind profile influences the turbulence structure. Between towers T3 and T4, we observe a slight decrease in the horizontal fluctuations (σ_u and σ_v , Fig. 12d, k). Within the trunk space, the values of Sk_w and Sk_u decrease, which denotes a decrease in the relative occurrence of large eddies. In contrast, within the canopy, the increasing value of Sk_w indicates an intensification of large vertical movements; Sk_u seems to be already adjusted within the canopy at tower T3 but significantly exceeds the typical value of 0.5 (Raupach et al. 1996; Finnigan 2000). This reveals that coherent structures shape the turbulent exchange within the top canopy ranges ($z \approx 0.8 h$) with an increasing eddy-penetration depth between towers T3 and T4. The particularly good correlation between u and w (Fig. 12j) supports this assessment.

The flow within the trunk space While passing the canopy vertically, turbulent structures appear to dissipate quickly. Figure 12b and g show that the mean level of momentum absorption (defined by $\overline{u'w'}/2$, Shaw et al. 1988) coincides with the peak of Sk_u at 25 m. Below a height of 20 m, the standard deviations and skewness decrease to relatively low values. The kurtosis profiles of both horizontal wind speed components ($Kurt_{u,v}$, not shown here) resemble the shape of the Sk_u profile but not the $Kurt_w$ in Fig. 12l. As a measure of the ‘peakedness’, the maxima are located at heights similar to Sk_w within the canopy; however, they exhibit an additional peak within the trunk space at 2 m. This indicates that the vertical (but not the horizontal) exchange is marked by either very strong vertical movement or no

vertical movement. Figure 12j reveals the fundamental difference between the flow above and below the canopy; the flow within the trunk space is marked by weak turbulence and a lack of correlation between u and w .

Like Dupont et al. (2011), we found a small upward momentum flux ($\overline{u'w'} > 0$) at tower T4 created by a decoupled sub-canopy wind, but unlike those authors, we observe no negative Sk_u values. Additionally, the negative w_n within the top layers of the canopy and the increase in u_n between towers T3 and T4 indicates a non-turbulent source of momentum for the flow within the trunk space. Figure 10 supports this assumption because the breakdown of the in-canopy flow for lower wind speeds is accompanied with a reduced or even positive w_n (i.e., less vertical advection). These observations represent an additional deviation from previous studies that report positive vertical winds below the canopy and mostly decreasing horizontal wind speeds within the trunk space (e.g., Yang et al. 2006a; Dupont and Brunet 2008).

Impact on scalar fluxes The pattern of the mean vertical velocities in Fig. 4 indicates that, within the canopy, the vertical exchange increases, but the horizontal transport is channelized. In Fig. 12d, f and k, the standard deviations σ_u and σ_w , as integral turbulence measures, show a stronger suppression of the horizontal motion than of vertical motion within the coniferous canopy. This creates anisotropy in the turbulence similar to unstable stratification and presumably increases the vertical exchange of scalars within the canopy. The horizontal relaxation of the flow within the open trunk space and the limitation of vertical movements near the ground changes the relationship between σ_u and σ_w , and we observe a suppressed vertical exchange.

These findings confirm the large-eddy simulation results of Dupont et al. (2011) and highlight the difference from the homogeneous stands reported in Brunet et al. (1994), where σ_u decreases continuously with stand depth. The change in the mechanical forced mixing by the canopy structure is often accompanied by a change in the buoyancy force within the canopy. Thus, it has important implications for the coupling of the ground-level air with the air stream above the canopy.

8.3 Momentum Budget

Mean momentum budget equation for forests The heterogeneous absorption of momentum by the vegetation modulates the wind field. Therefore, an important objective of the experiment was the assessment of the momentum transfer within the canopy and its parametrization (Queck et al. 2012). Under steady-state conditions, neglecting the Coriolis force and buoyancy effect, the conservation of the streamwise component of momentum can be written as,

$$0 = \bar{u} \frac{\partial \bar{u}}{\partial x} + \bar{v} \frac{\partial \bar{u}}{\partial y} + \bar{w} \frac{\partial \bar{u}}{\partial z} + \frac{\partial \overline{u'u'}}{\partial x} + \frac{\partial \overline{u'v'}}{\partial y} + \frac{\partial \overline{u'w'}}{\partial z} + \frac{1}{\rho} \frac{\partial \bar{p}}{\partial x} + \frac{F_{D,x}}{\rho} \quad (2)$$

where x, y, z denote the west, north and vertical, respectively, in a rectangular coordinate system, ρ is the air density, p is the air pressure and $F_{D,x}$ represents the drag force in the x direction. The first three terms on the right-hand side of Eq. 2 represent the advective transport and the second three terms the relevant terms of the kinematic flux tensor (also, the Reynolds-stress tensor), followed by the pressure gradient force and the drag force. One of the issues is as follows: what are the relevant terms in Eq. 2 in a transect across a clearing?

Kinematic gradients For a flow that is homogeneous along the lateral direction, the sonic array permits us to estimate key terms in the streamwise (and vertical) mean momentum

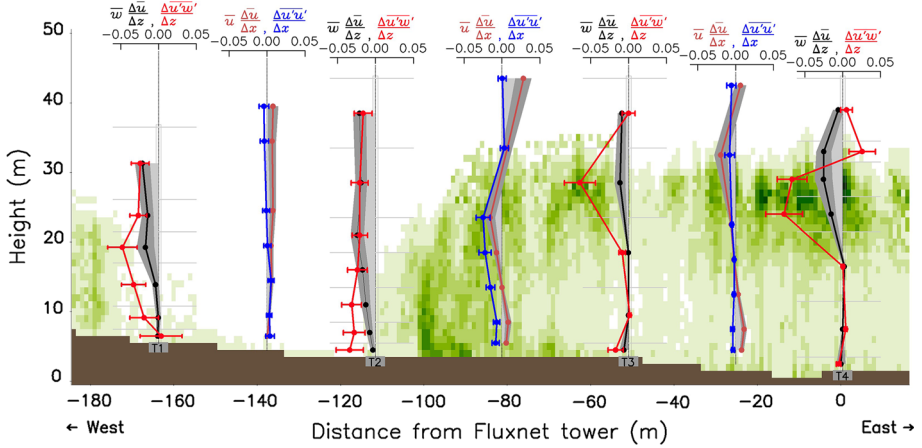


Fig. 13 Profiles of the horizontal acceleration by vertical advection (*black*) and vertical kinematic stress (*red*) at the towers, and by horizontal advection (*brown*) and horizontal kinematic stress (*blue*) between the towers. The standard deviation is indicated by *error bars* for the turbulent fluxes and by *dark grey shading* for the advective fluxes

balances. The fraction of streamwise component of momentum that is introduced by the crosswise air movement could only be measured within the lowest layer (2 m) around tower T4 by the sonics from position M8 and M9 (see Fig. 2). The averages over all 30-min values result in $\bar{v}\partial\bar{u}/\partial y = -0.0008 \text{ m s}^{-2}$ and $\partial\bar{u}'v'/\partial y = -0.0012 \text{ m s}^{-2}$, which are at least ten times smaller than $\bar{u}\partial\bar{u}/\partial x$ or $\partial\bar{u}'w'/\partial z$ in this area.

Figure 13 shows the streamwise component of momentum carried in by vertical and streamwise air movements inferred from the sonic measurements (terms 1, 3, 4 and 6 in Eq. 2). The profile plots of the gradients are placed between the related sonic positions. Note that negative values indicate a loss of momentum for the respective term, i.e., a transfer into other terms of Eq. 2 within the indicated compartment. Accordingly, positive values indicate a transfer of momentum from other terms into the respective term. The following points characterize the figure of the momentum exchange:

- The vertical turbulent momentum import $\partial\bar{u}'w'/\partial z$ dominates the flow over the clearing as well as within the crown space. It is obviously the main source for the drag on the vegetation ($F_{D,x}$).
- Above the clearing, the momentum entry from $\bar{w}\partial\bar{u}/\partial z$ and $\partial\bar{u}'w'/\partial z$ is not balanced by an acceleration of air ($\bar{u}\partial\bar{u}/\partial z$). Because there is no absorption of momentum by the trees, we assume an increase in $\partial\bar{p}/\partial x$.
- The gradient $\partial\bar{u}'w'/\partial z$ shows a local maxima at a height of 20 m around tower T1, which is likely a result of flow separation (i.e., occasional recirculation) behind the forest edge.
- The horizontal kinematic stress $u'u'$ changes only between towers T2 and T3, and so the turbulence intensity within the vegetation layer seems to adjust quickly after changes in vegetation structure.
- The momentum added by the deceleration of the air at the peripheral zones of the canopy ($\bar{u}\partial\bar{u}/\partial x < 0$) is likely absorbed by the drag of the canopy. Furthermore, it feeds air into the canopy (see the divergence of the vertical wind in Figs. 10 or 12), supporting the acceleration of the air within the trunk space.

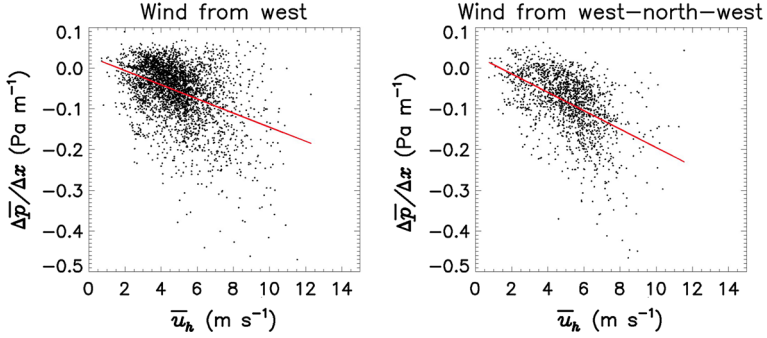


Fig. 14 Local pressure gradient between the forest edge and the trunk space measured between $x = -113$ m and $x = -23$ m. The *red line* indicates the linear regression of $\Delta p/\Delta x$ with respect to wind speed. The *left* plot shows the gradient for winds in line with the investigated transect ($\overline{u}_h = \overline{u}$), and the *right* plot the gradient for winds from north-west (i.e., perpendicular to the forest edge, see Fig. 1)

- The vertical advection of streamwise component of momentum is limited by \overline{w} . Although, the profile of $\partial\overline{u}/\partial z$ is very similar between towers T3 and T4 (see Fig. 12a), the negative \overline{w} causes a much higher momentum transfer in the tree crowns around tower T4.
- An interesting feature is again the positive $\partial\overline{u}'w'/\partial z$ values directly above the tree crowns at tower T4. Now, the possible source of momentum is visible due to the negative $\overline{w}\partial\overline{u}/\partial z$. We assume that this source increases the Reynolds stress directly above the canopy within layers where the additional turbulent momentum is not absorbed by the canopy.
- The acceleration of the air below the canopy ($\overline{u}\partial\overline{u}/\partial x > 0$) is balanced by the turbulent momentum entry at the forest edge between towers T2 and T3. However, between towers T3 and T4, neither the turbulent nor the advective terms provide momentum input. Thus, we conclude that the gain is caused by the pressure term.

Pressure gradient The numerical results of Dupont et al. (2011) indicated that, in addition to the advective transport of momentum, the local pressure gradient may also add a significant contribution to the momentum balance. Consequently, we examined the pressure gradient at the forest edge from 22 November 2011, until 22 May 2012 (the set-up is described in Sect. 4). Unfortunately, this realization took place after the intensive measurement period between 2008 and 2009 had finished. Due to this postponement, the results cannot be combined directly with the wind measurements.

Although we observed a large data scatter (Pearson correlation coefficient $r = 0.40$), Fig. 14 reveals the existence of a negative local pressure gradient that increases with wind speed. The regression of \overline{u} on $\Delta p/\Delta x$ yields a value of $-0.017 \text{ kg s}^{-1} \text{ m}^{-3}$. The correlation is stronger ($r = 0.50$) for flow perpendicular to the forest edge, i.e., for flow from the west-north-west (Fig. 14 right side). The pressure gradient changes by $-0.023 \text{ kg s}^{-1} \text{ m}^{-3}$ times \overline{u} , and a westerly wind of $\overline{u} \approx 4 \text{ m s}^{-1}$ above the canopy would result in an acceleration of the air within the canopy by $\partial\overline{p}/\partial x/\rho \approx 0.07 \text{ m s}^{-2}$ due to pressure forces. Reviewing Figs. 10 and 12 (note that these data are normalized with the reference velocity), we obtain only $\Delta\overline{u} \approx 0.75 \text{ m s}^{-1}$ between towers T2 and T4 within the trunk space. Thus, the majority of the acceleration due to the pressure gradient is likely absorbed by the drag in the canopy and on the ground.

The model of Finnigan and Belcher (2004) predicts increasing local pressure on the lee side of a shallow hill. Assuming a similar effect, the *S-Berg* hillock to the west of the site

likely moderates the measured pressure gradient and causes some of the scatter within the measurements. The results show that, around the clearing, all terms of the Eq. 2 change in comparable magnitude and none should be neglected. The importance of the single terms varies within the roughness layer; in other words, they are controlled by the canopy structure.

9 Synopsis

We have described field measurements from the TurbEFA project that were made at the *Fluxnet* site *Tharandt* and a nearby forest clearing. The prominent features of the experiment are the simultaneously recorded wind measurements using 27 ultrasonic anemometers on four towers and five 2-m masts over one year and the terrestrial laser scans of the vegetation.

9.1 Data Basis

Vegetation Structure In the momentum equation, displacement and friction are the two main effects of vegetation cover on the airflow near the surface. Using terrestrial laser-scanning methods, we obtained a three-dimensional vegetation model with a resolution of 1 m^3 , which is suitable for numerical models and enables us to analyze the turbulence measurements with regard to the flow obstacles (e.g., in [Queck et al. 2012](#)). The investigated stand is dominated by evergreen plants (almost 90 %). Although measurements of the spring flushing revealed a temporary 25 % increase in *PAI* values, the measured mean velocities within the canopy are hardly influenced by the phenological phases.

Vertical Velocity The instrumental bias in the measurements of the vertical wind component is important but difficult to determine because the vertical velocity is very small compared to the bias. Considering measurements over or even within heterogeneous canopies, the application of the planar fit method can lead to serious errors. Instead of fitting a plane to the whole dataset, we performed sector-wise fitting but subsequently averaged the offsets of all sectors.

As a result, the comparison of the earlier WinCanop experiment with the TurbEFA experiment revealed a close conformity of the vertical profiles of the wind statistics, despite the changes in the set-up between the experiments. In addition to the reproducibility of the results, this shows the spatial representativeness of the measurements and the persistence of the mean flow characteristics over time.

Classification of the Data A key issue in the data analysis is the classification of the measurements according to meteorological conditions. In one case, averaging over larger ranges of environmental conditions may reduce the influence of very specific flow situations around a sensor within the canopy, thus increasing the spatial representativeness. For example, within the crown space, averages over a wind sector of 30° have a higher spatial representativeness than averages over a 5° wind sector. In another case, the specific effects of turbulent flow, such as the recirculation in the clearing, cannot be observed in averages over all wind-speed classes. The irregular onset of flow patterns, such as the recirculation on the investigated forest clearing, produces uncertainty in the wind statistics. Thus, the application of narrow wind-speed classes but also stationary meteorological conditions for periods longer than 30 min reduces the scatter of field measurements around class mean values.

During the TurbEFA experiment, we recorded data for approximately 7550 h. However, after applying the constraints of the ‘standard case’ (defined in Table 1), only 126 h of data

remain for the comparison with the numerical simulations and with data from a wind-tunnel experiment (see [Queck et al. 2015](#)). This is yet another illustration of the fact that long-term field experiments are necessary to obtain statistically reliable datasets for comparison with numerical models.

9.2 Aerodynamic Coupling of the Trunk Space

Development of a Sub-Canopy Wind-Speed Maximum The investigations of the flow passing edges of horizontally homogeneous but vertically structured forests in [Dupont et al. \(2011\)](#) showed an advective momentum entry into the trunk space at the edge, followed by a deceleration, producing a vertical wind upward through the canopy. The hypothesis that this is also the case for a more heterogeneous forest with small clearings has to be rejected after our observations. The TurbEFA experiment shows low horizontal wind speeds directly downstream of the forest edge but an acceleration of the flow over the first 100 m within the trunk space, which is supported by a vertical wind downward through the canopy. The simulations of [Damschen et al. \(2014\)](#) showed similar flow patterns.

However, this sub-canopy flow is not observed for low horizontal wind speeds. The flow regime in the clearing and within the canopy appears to switch at a threshold of $\overline{u}_h(42 \text{ m}) \approx 1.5 \text{ m s}^{-1}$. In cases with lower horizontal wind speed, a recirculation zone develops over the clearing and the trunk space is barely ventilated. With increasing wind speed, the pressure on the windward forest edge increases, and the air penetrates the dense vegetation there. Coincidentally, the recirculation zone shrinks to a smaller range at the leading edge of the forest clearing.

Effect of the Pressure Gradient Because the vertical momentum entry (both turbulent and advective) is almost completely absorbed within the canopy and no other source of momentum occurs between towers T3 and T4, the acceleration of the sub-canopy air is driven by the local pressure gradient. The development of the pressure gradient with increasing wind speed, in combination with the intermittent recirculation on the clearing, is obviously the reason for the non-linear dynamic of the airflow within the trunk space.

Based on the decoupling of the airflow within the trunk space, it follows that the Coriolis force is small and the large-scale pressure gradient has a stronger influence on the wind direction ([Wilson and Flesch 1999](#)).

Effect of Turbulence and Coherent Structures The exchange between the canopy and the air above the canopy is characterized by occasional stronger sweeps, which are indicated by a skewness clearly greater than one. However, it is questionable whether these sweeps reach the lower layers of the stand. The correlation between \overline{u} and \overline{w} ceases below 20 m and the vertical momentum transfer changes its sign, and consequently the trunk space is mostly decoupled from the flow above. The exchange between trunk space and the air above is reduced to gaps in the canopy like clearings and forest paths.

9.3 Implications for the Exchange of Mass and Energy

Exchange at Gaps in the Forest Canopy We assume that the small gaps in the canopy around towers T3 and T4 deflect the flow downward and have a similar effect as the clearing. The depth of the penetration likely scales with the size of the respective clearing. Under windy conditions, clearings wider than the canopy height are completely coupled with the atmosphere above (which is not necessarily true under calm and stable conditions).

Turbulent Exchange with the Canopy Vertical fluctuations are less obstructed by the canopy structure of the coniferous stand than horizontal fluctuations. This allows us to assume that turbulent exchange of mass and energy in the horizontal and vertical directions are substantially different within the canopy compared to the sub-layers above and below.

9.4 Influence of the Topography

Tethered balloon soundings and systematic alterations in wind-direction distributions indicate an influence of the *S-Berg* hillock on the topmost measurements of the transect. However, the small forest units of the area, which are interrupted by clearings and forest paths, create a high background surface roughness (see Fig. 11). Thus, the influence of the *S-Berg* hillock is not detectable in the measurements below a height of $1.5h$.

10 Concluding Remarks

The dynamics of the turbulent flow are clearly influenced by the local vegetation structure. Mechanisms that are observed at homogeneous sites do not explain important features at heterogeneous sites. Clearings deflect the flow downwards and feed the sub-canopy flow according to the wind speed and, likely, clearing size. Local pressure gradients play an important role in the development of sub-canopy flow.

The flow within the investigated coniferous stand can be divided into two layers, the flow in the upper part of the canopy, which interacts with the atmosphere above via intermittent episodes of stronger turbulence, and the trunk space, which is mostly decoupled from the flow above depending on the exchange via small clearings and forest roads. Consequently, large horizontal shifts in trace gases originating from soil and understorey are possible within the stand.

Combining meteorological measurements with high-resolution vegetation information in numerical models allows the interpolation of the measurements on a physical basis. This gives further insight into the mechanism of the exchange between atmosphere and surface and can lead to new approaches for the determination of the surface fluxes that also include advective fluxes.

The presented turbulence measurements from various sensor locations, additional temperature and radiation measurements, as well as precise vegetation information from terrestrial (and airborne) laser scanning, provide a database to test and improve numerical models.

Acknowledgments The work was supported by the German National Science Foundation (Deutsche Forschungsgemeinschaft, DFG) within the priority programme SPP 1276, ‘*Multiple Scales in Fluid Mechanics and Meteorology*’ (MetStröm) within the project ‘Turbulent Exchange processes between Forested areas and the Atmosphere’. We thank Dr. Christian Feigenwinter and Dr. Roland Vogt (University of Basel) for their logistical support and scientific discussions and we thank the staff of the Chair of Meteorology of the TU Dresden, namely Uwe Eichelmann, Heiko Prasse and Markus Hehn for technical support.

References

- Albertson JD, Katul GG, Wiberg P (2001) Relative importance of local and regional controls on coupled water, carbon, and energy fluxes. *Adv Water Resour* 24(9–10):1103–1118
- Aubinet M (2008) Eddy covariance CO₂ flux measurements in nocturnal conditions: an analysis of the problem. *Ecol Appl* 18(6):1368–1378

- Aubinet M, Vesala T, Papale D (eds) (2012) Eddy covariance: a practical guide to measurement and data analysis, 2012th edn. Springer, Dordrecht, 460 pp
- Baldocchi D, Falge E, Gu L, Olson R, Hollinger D, Running S, Anthoni P, Bernhofer C, Davis K, Evans R, Fuentes J, Goldstein A, Katul G, Law B, Lee X, Malhi Y, Meyers T, Munger W, Oechel W, Paw KT, Pilegaard K, Schmid HP, Valentini R, Verma S, Vesala T, Wilson K, Wofsy S (2001) FLUXNET: a new tool to study the temporal and spatial variability of ecosystem-scale carbon dioxide, water vapor, and energy flux densities. *Bull Am Meteorol Soc* 82(11):2415–2434
- Banerjee T, Katul G, Fontan S, Poggi D, Kumar M (2013) Mean flow near edges and within cavities situated inside dense canopies. *Boundary-Layer Meteorol* 149(1):19–41
- Belcher SE, Finnigan JJ, Harman IN (2008) Flows through forest canopies in complex terrain. *Ecol Appl* 18(6):1436–1453
- Belcher SE, Harman IN, Finnigan JJ (2012) The wind in the willows: flows in forest canopies in complex terrain. *Annu Rev Fluid Mech* 44(1):479–504
- Bernhofer C, Aubinet M, Clement R, Grelle A, Grünwald T, Ibrom A, Jarvis P, Rebmann C, Schulze ED, Tenhunen JD (2013) Spruce forests (Norway and Sitka Spruce, Including Douglas fir): carbon and water fluxes and balances, ecological and ecophysiological determinants. *Ecological studies*, vol 163. Springer, Berlin, pp 99–123
- Bernhofer C, Grünwald T, Spank U, Clausnitzer F, Eichelmann U, Feger KH, Köstner B, Prasse H, Menzer A, Schwärzel K (2011) Mikrometeorologische, pflanzenökologische und bodenhydrologische Messungen in Buchen- und Fichtenbeständen des Tharandter Waldes. *Waldökol Landsch Nat* 12:17–28
- Bienert A, Maas HG (2009) Methods for the automatic geometric registration of terrestrial laser scanner point clouds in forest stands. *IAPRS* 38-3/W8:1–6
- Bienert A, Queck R, Schmidt A, Bernhofer C, Maas HG (2010) Voxel space analysis of terrestrial laser scans in forests for wind field modelling. *IAPRS* 38(Part 5):92–97
- Bohrer G, Katul GG, Walko RL, Avissar R (2009) Exploring the effects of microscale structural heterogeneity of forest canopies using large-eddy simulations. *Boundary-Layer Meteorol* 132(3):351–382
- Brunet Y, Finnigan JJ, Raupach MR (1994) A wind tunnel study of air flow in waving wheat: single-point velocity statistics. *Boundary-Layer Meteorol* 70(1):95–132
- Cassiani M, Katul GG, Albertson JD (2008) The effects of canopy leaf area index on airflow across forest edges: large-eddy simulation and analytical results. *Boundary-Layer Meteorol* 126(3):433–460
- Damschen EI, Baker DV, Bohrer G, Nathan R, Orrock JL, Turner JR, Brudvig LA, Haddad NM, Levey DJ, Tewksbury JJ (2014) How fragmentation and corridors affect wind dynamics and seed dispersal in open habitats. *Proc Natl Acad Sci USA* 111(9):3484–3489
- Detto M, Katul GG, Siqueira M, Juang J, Stoy P (2008) The structure of turbulence near a tall forest edge: the backward-facing step flow analogy revisited. *Ecol Appl* 18(6):1420–1435
- Dupont S, Brunet Y (2008) Edge flow and canopy structure: a large-eddy simulation study. *Boundary-Layer Meteorol* 126(1):51–71
- Dupont S, Bonnefond JM, Irvine MR, Lamaud E, Brunet Y (2011) Long-distance edge effects in a pine forest with a deep and sparse trunk space: in situ and numerical experiments. *Agric For Meteorol* 151(3):328–344
- Eysn L, Pfeifer N, Ressler C, Hollaus M, Grafl A, Morsdorf F (2013) A practical approach for extracting tree models in forest environments based on equirectangular projections of terrestrial laser scans. *Remote Sens* 5(11):5424–5448
- Feigenwinter C, Bernhofer C, Vogt R (2004) The influence of advection on the short term CO₂-budget in and above a forest canopy. *Boundary-Layer Meteorol* 113(2):201–224
- Feigenwinter C, Bernhofer C, Eichelmann U, Heinesch B, Hertel M, Janous D, Kolle O, Lagergren F, Lindroth A, Minerbi S, Moderow U, Mölder M, Montagnani L, Queck R, Rebmann C, Vestin P, Yernaux M, Zeri M, Ziegler W, Aubinet M (2008) Comparison of horizontal and vertical advective CO₂ fluxes at three forest sites. *Agric For Meteorol* 148(1):12–24
- Finnigan JJ (2000) Turbulence in plant canopies. *Annu Rev Fluid Mech* 32:519–571
- Finnigan JJ, Belcher SE (2004) Flow over a hill covered with a plant canopy. *Q J R Meteorol Soc* 130(596):1–29
- Fleisch TK, Wilson JD (1999) Wind and remnant tree sway in forest cutblocks. I. Measured winds in experimental cutblocks. *Agric For Meteorol* 93(4):229–242
- Foken T, Aubinet M, Finnigan JJ, Leclerc MY, Mauder M, Paw U KT (2011) Results of a panel discussion about the energy balance closure correction for trace gases. *Bull Am Meteorol Soc* 92(4):ES13–ES18
- Fontan S, Katul GG, Poggi D, Manes C, Ridolfi L (2012) Flume experiments on turbulent flows across gaps of permeable and impermeable boundaries. *Boundary-Layer Meteorol* 147(1):21–39
- Frank C, Ruck B (2008) Numerical study of the airflow over forest clearings. *Forestry* 81(3):259–277

- Frühauf C, Zimmermann L, Bernhofer C (1999) Comparison of forest evapotranspiration from ECEB-measurements over a spruce stand with the water budget of a catchment. *Phys Chem Earth Part B* 24(7):805–808
- Gash JHC (1986) Observations of turbulence downwind of a forest–heath interface. *Boundary-Layer Meteorol* 36(3):227–237
- Gavrilov K, Accary G, Morvan D, Lyubimov D, Méradji S, Bessonov O (2010) Numerical simulation of coherent structures over plant canopy. *Flow Turbul Combust* 86(1):89–111
- Grünwald T, Bernhofer C (2007) A decade of carbon, water and energy flux measurements of an old spruce forest at the Anchor Station Tharandt. *Tellus B* 59:387–396
- Högström U, Smedman AS (2004) Accuracy of sonic anemometers: laminar wind-tunnel calibrations compared to atmospheric in situ calibrations against a reference instrument. *Boundary-Layer Meteorol* 111(1):33–54
- Huang J, Cassiani M, Albertson JD (2011) Coherent turbulent structures across a vegetation discontinuity. *Boundary-Layer Meteorol* 140(1):1–22
- Irvine MR, Gardiner BA, Hill MK (1997) The evolution of turbulence across a forest edge. *Boundary-Layer Meteorol* 84(3):467–496
- Jegadee OO, Foken T (1999) A study of the internal boundary layer due to a roughness change in neutral conditions observed during the LINEX field campaigns. *Theor Appl Climatol* 62(1–2):31–41
- Kanani-Sühring F, Raasch S (2015) Spatial variability of scalar concentrations and fluxes downstream of a clearing-to-forest transition: a large-eddy simulation study. *Boundary-Layer Meteorol* 155(1):1–27
- Lee X (2000) Air motion within and above forest vegetation in non-ideal conditions. *For Ecol Manag* 135(1–3):3–18
- Lee X, Finnigan JJ, Paw U KT (2004) Coordinate systems and flux bias error. In: Massman W, Law B (eds) *Handbook of micrometeorology*, 1st edn. Kluwer, Dordrecht, pp 33–36
- Liu J, Chen JM, Black TA, Novak MD (1996) E– ϵ modelling of turbulent air flow downwind of a model forest edge. *Boundary-Layer Meteorol* 77(1):21–44
- Maurer KD, Bohrer G, Kenny WT, Ivanov VY (2015) Large-eddy simulations of surface roughness parameter sensitivity to canopy-structure characteristics. *Biogeosciences* 12(8):2533–2548
- Moderow U, Bernhofer C (2014) Cluster of the technische universität dresden for greenhouse gas and water fluxes. In: iLEAPS Special Newsletter issue on Environmental Research Infrastructures, pp 34–37
- Moderow U, Feigenwinter C, Bernhofer C (2007) Estimating the components of the sensible heat budget of a tall forest canopy in complex terrain. *Boundary-Layer Meteorol* 123(1):99–120
- Nakai T, van der Molen M, Gash J, Kodama Y (2006) Correction of sonic anemometer angle of attack errors. *Agric For Meteorol* 136(1–2):19–30
- Nishiyama RT, Bedard AJ (1991) A ‘Quad-Disc’ static pressure probe for measurement in adverse atmospheres: with a comparative review of static pressure probe designs. *Rev Sci Instrum* 62(9):2193–2204
- Otto M (2005) Vergleich unterschiedlicher Verfahren zur Abschätzung der Kohlenstoffspeicherung in einem Fichtenwald. Diplomarbeit, TU Dresden, Tharandt, 81 pp
- Patton EG, Horst TW, Sullivan PP, Lenschow DH, Oncley SP, Brown WOJ, Burns SP, Guenther AB, Held A, Karl T, Mayor SD, Rizzo LV, Spassler SM, Sun J, Turnipseed AA, Allwine EJ, Edburg SL, Lamb BK, Avissar R, Calhoun RJ, Kleissl J, Massman WJ, Paw U KT, Weil JC (2011) The canopy horizontal array turbulence study (CHATS). *Bull Am Meteorol Soc* 92:593–611
- Prescher AK, Grünwald T, Bernhofer C (2010) Land use regulates carbon budgets in eastern Germany: from NEE to NBP. *Agric For Meteorol* 150(7–8):1016–1025
- Queck R, Bienert A, Maas HG, Harmansa S, Goldberg V, Bernhofer C (2012) Wind fields in heterogeneous conifer canopies: parameterisation of momentum absorption using high-resolution 3D vegetation scans. *Eur J For Res* 131(1):165–176
- Queck R, Bernhofer C, Bienert A, Eipper T, Goldberg V, Harmansa S, Hildebrand V, Maas HG, Schlegel F, Stiller J (2015) TurbEFA: an interdisciplinary effort to investigate the turbulent flow across a forest clearing. *Meteorol Z* 6:637–659
- Raupach MR, Thom AS (1981) Turbulence in and above plant canopies. *Annu Rev Fluid Mech* 13:97–129
- Raupach M, Bradley EF, Ghadiri H (1987) A wind tunnel investigation into aerodynamic effect of forest clearings on the nesting of Abbott’s booby on Christmas Island. Tech. Rep., CSIRO Centre for Environmental Mechanics, Canberra, 23 pp
- Raupach MR, Finnigan JJ, Brunet Y (1996) Coherent eddies and turbulence in vegetation canopies: the mixing-layer analogy. *Boundary-Layer Meteorol* 78(3):351–382
- Rebmann C, Göckede M, Foken T, Aubinet M, Aurela M, Berbigier P, Bernhofer C, Buchmann N, Carrara A, Cescatti A, Ceulemans R, Clement R, Elbers JA, Granier A, Grünwald T, Guyon D, Havránková K, Heinesch B, Knohl A, Laurila T, Longdoz B, Marcolla B, Markkanen T, Miglietta F, Moncrieff J, Montagnani L, Moors E, Nardino M, Ourcival JM, Rambal S, Rannik U, Rotenberg E, Sedlak P,

- Unterhuber G, Vesala T, Yakir D (2005) Quality analysis applied on eddy covariance measurements at complex forest sites using footprint modelling. *Theor Appl Climatol* 80(2–4):121–141
- Rudnicki M, Mitchell SJ, Novak MD (2004) Wind tunnel measurements of crown streamlining and drag relationships for three conifer species. *Can J For Res* 34(3):666–676
- Schlegel F, Stiller J, Bienert A, Maas HG, Queck R, Bernhofer C (2012) Large-eddy simulation of inhomogeneous canopy flows using high resolution terrestrial laser scanning data. *Boundary-Layer Meteorol* 142:223–243
- Schlegel F, Stiller J, Bienert A, Maas HG, Queck R, Bernhofer C (2015) Large-eddy simulation study of the effects on flow of a heterogeneous forest at sub-tree resolution. *Boundary-Layer Meteorol* 154(1):27–56
- Schwärzel K, Menzer A, Clausnitzer F, Spank U, Häntzschel J, Grünwald T, Köstner B, Bernhofer C, Feger KH (2009) Soil water content measurements deliver reliable estimates of water fluxes: a comparative study in a beech and a spruce stand in the Tharandt forest (Saxony, Germany). *Agric For Meteorol* 149(11):1994–2006
- Serafimovich A, Thomas C, Foken T (2011) Vertical and horizontal transport of energy and matter by coherent motions in a tall spruce canopy. *Boundary-Layer Meteorol* 140(3):429–451
- Shaw R, Patton E (2003) Canopy element influences on resolved- and subgrid-scale energy within a large-eddy simulation. *Agric For Meteorol* 115:5–17
- Shaw R, den Hartog G, Neumann H (1988) Influence of foliar density and thermal stability on profiles of Reynolds stress and turbulence intensity in a deciduous forest. *Boundary-Layer Meteorol* 45:391–409
- Sogachev A, Leclerc MY, Zhang G, Rannik I, Vesala T (2008) CO₂ fluxes near a forest edge: a numerical study. *Ecol Appl* 18(6):1454–1469
- Vosselman G, Maas HG (2010) *Airborne and terrestrial laser scanning*. Whittles Publishing, Dunbeath, 336 pp
- Wilson JD, Flesch TK (1999) Wind and remnant tree sway in forest cutblocks. III. A windflow model to diagnose spatial variation. *Agric For Meteorol* 93(4):259–282
- Yang B, Morse A, Shaw R, Paw U KT (2006a) Large-eddy simulation of turbulent flow across a forest edge. Part II: momentum and turbulent kinetic energy budgets. *Boundary-Layer Meteorol* 121:433–457
- Yang B, Raupach MR, Shaw RH, Paw U KT, Morse A (2006b) Large-eddy simulation of turbulent flow across a forest edge. Part I: flow statistics. *Boundary-Layer Meteorol* 120(3):377–412
- Yi C (2008) Momentum transfer within canopies. *J Appl Meteorol Climatol* 47(1):262–275